
VARIABILITY AND THERMAL MODULATION OF LOCOMOTOR STATISTICS IN ZEBRAFISH

Guillaume Le Goc¹ Sophia Karpenko^{1,2} Volker Bormuth¹ Raphaël Candelier¹

Georges Debrégeas^{1,3,*}

¹ Sorbonne Université, CNRS, Institut de Biologie Paris-Seine (IBPS), Laboratoire Jean Perrin (LJP), Paris, France;

² Université Paris Sciences et Lettres, Paris, France;

³ Lead contact.

* Correspondence : georges.debregeas@sorbonne-universite.fr

March 17, 2021

Summary

1 Variability is a hallmark of animal behavior. It endows individuals and populations with the
2 capacity to adapt to ever-changing conditions. How variability is internally regulated and
3 modulated by external cues remains elusive. Here we address this question by focusing on
4 the exploratory behavior of zebrafish larvae as they freely swim at different, yet ethologically
5 relevant, water temperatures. We show that, for this simple animal model, five short-term
6 kinematic parameters together control the long-term exploratory dynamics. We establish
7 that the bath temperature consistently impacts the means and variances of these parameters,
8 but leave their pairwise covariance unchanged. These results indicate that the temperature
9 merely controls the sampling statistics within a well-defined accessible locomotor repertoire.
10 At a given temperature, the exploration of the behavioral space is found to take place over
11 tens of minutes, suggestive of a slow internal state modulation that could be externally biased
12 through the bath temperature. By combining these various observations into a minimal
13 stochastic model of navigation, we show that this thermal modulation of locomotor kinematics
14 results in a thermophobic behavior, complementing direct gradient-sensing mechanisms.

15 **Keywords** behavior · variability · thermokinesis · zebrafish · navigation · locomotion

16 **1 Introduction**

17 Variability, both inter- and intra-individual, is an ubiquitous trait of animal behavior [1]. Intra-individual
18 variability may participate in efficient strategies, as best exemplified by the alternation of exploration and
19 exploitation phases during foraging [2, 3]. It can also endow the animal, or the population, with robustness,
20 *i.e.* the ability to rapidly and efficiently cope with changing environmental conditions [4, 5]. The idea, known
21 as bet-hedging, is that a modest loss in fitness associated with phenotypic variability could be balanced by
22 the gain in leniency when facing unexpected and possibly hostile conditions. The origin of inter-individual
23 variability may be attributed to genetic, epigenetic or developmental differences. Intra-individual variability
24 may in turn reflect spontaneous transitions between distinct brain states, *i.e.* patterns of persistent neural
25 activity [6, 7]. It may also be the signature of endogenous modulations in the production of neuromodulators
26 [8].

27 Although the functional significance of variability in animal behavior is now largely recognized [9], the way it
28 is regulated and modulated by external cues, as well as its neuronal substrate remain elusive. To address
29 this question, one not only needs to quantify variability, but also manipulate it in a physiologically relevant
30 manner, in an animal that is accessible to both behavioral and neuronal circuit interrogation. Here we used
31 the zebrafish larva as a model vertebrate as it is uniquely amenable to *in vivo* whole brain functional imaging
32 [10–12] and to high-throughput behavioral studies [13, 14].

33 As an ectothermic animal, zebrafish must actively navigate towards regions of its environment that are
34 thermally optimal for its thriving [15], while potentially being exposed to a wide range of temperatures [16].
35 How fish swim in thermal gradients has been extensively studied [17], and the neuronal circuits underlying
36 this thermotactic process have been identified [18]. Zebrafish larvae integrate thermal signals (change in
37 temperature) over a sub-second time window, and adapt their forthcoming movement accordingly in order to
38 eventually move towards optimal zones.

39 Here we focus on the exploratory dynamics at various but spatially uniform temperatures. We use a reductive
40 approach, as previously introduced [19], to quantify its spontaneous locomotion using a finite number of
41 short-term kinematic parameters. We then quantify how the bath temperature not only impacts the mean
42 of these parameters, but also their statistical distribution (variability) and pairwise covariance. We further
43 assess the time-scale over which this behavioral variability unfolds at the level of individual animals. From
44 this detailed analysis, we build a numerical model of zebrafish larvae navigation at all temperatures over
45 the physiologically relevant range. Finally, we use this model to demonstrate how this thermal adaptation
46 of spontaneous swimming pattern may complement the thermotactic mechanism, based on direct gradient
47 sensing, in order for the animal to limit its presence in potentially harmful environments.

48 **2 Results**

49 **A behavioral assay to record spontaneous navigation at different temperatures.**

50 Batches of 10 zebrafish larvae aged 5-7 days were video-monitored at 25 frames/second for periods of 30
51 minutes as they freely swam in a rectangular $100 \times 45 \times 4.5 \text{mm}^3$ pool at a constant and uniform temperature

MARCH 17, 2021

52 (figure 1A, see Methods). For each batch, we successively imposed up to 5 values of temperature (18, 22, 26,
53 30 and 33°C) in a random order. This thermal range spans the non-lethal conditions for larval zebrafish, and
54 has been shown to be effectively encountered by the animal in its natural habitat [20]. Each 30 min-long
55 recording session was preceded by a 14 min-long period of habituation to allow the animals to reach their
56 steady-state exploratory regime. A total of 10 batches per temperature involving 170 different fish were used.

57 Larval zebrafish swim in discrete bouts lasting for about 100ms, interspersed with $\sim 1 - 2$ s periods of rest.
58 As we aim to probe how the bath temperature impacts the long-term exploratory process, we focus on the
59 characterization of a few kinematic parameters associated with each bout. We thus ignore the fine structure
60 of the swimming events, such as the amplitude of the tail deflection or beating frequency [21, 22], but examine
61 their resulting heading reorientation and linear displacements. The center of mass coordinates and orientation
62 of each larva in every frame were extracted using FastTrack [23] (see Methods). For each identified swim bout,
63 we computed three scalar parameters (Figure 2A) whose statistics control the fish spatio-temporal exploration
64 [19]: (i) the interbout interval (IBI), δt_n , is the idle time following the bout event, (ii) the displacement, d_n ,
65 is the travelled distance associated with the bout, and (iii) the reorientation angle, $\delta \theta_n$, denotes the change
66 in heading direction.

67 Tracking was performed within the innermost region of the arena, at a minimum distance of 5 mm from the
68 walls, as the latter would inevitably bias the exploration dynamics. As a result, individual fish were not
69 tracked continuously over the entire recording periods, but along *trajectories* (from one wall to another). In the
70 analysis, we ignored trajectories that last less than 25 seconds. Example trajectories for three temperatures
71 are shown in figure 1C, where each dot indicates the location of a swim bout, while its size reflects the
72 interbout interval. This comparison provides a first qualitative illustration of the effect of temperature on the
73 fish exploration. At low temperatures (18°C), the trajectories are relatively straight, comprising a majority of
74 small discrete forward bouts executed at relatively low frequency. At high temperatures, the trajectories
75 appear much more meandering, with more frequent and ample reorienting maneuvers with longer travelled
76 distances. In the following, we quantify these differences by systematically comparing the statistics of the
77 per-bout kinematic parameters at different temperatures.

78 **The bath temperature controls the statistical distributions of the kinematic parameters.**

79 For each batch and temperature, a probability density function (pdf) was computed for interbout intervals,
80 displacements and turn angles by pooling all bout events. We then computed an average distribution across
81 batches (figure 2B-D, respectively) for the 3 parameters, as well as the temperature-dependence of their mean
82 values (figure 2F-H).

83 A decrease in the bath temperature from 26°C to 18°C is associated with an increase of the mean IBI ($\langle \delta t \rangle$)
84 from 1 to 1.4s, while the bout frequency remains essentially unchanged at higher temperatures (2B, F). This
85 increase in the mean values is accompanied by a systematic broadening of the statistical distribution. The
86 per-bout displacement exhibits a similar trend (figure 2C). This quantity increases in the range 18-26°C from
87 1 to 1.5mm, and remains unchanged at higher temperatures (figure 2G).

88 The turn angle distributions shown in figure 2D reveal the existence of two main bout categories [13, 19,
89 24]. The central narrow peak corresponds to forward bouts while the wide tail is associated with turning
90 events. We adjusted this distribution as a sum of two empirically chosen functional forms in order to extract
91 the fraction of turning bouts p_{turn} (see Methods). This quantity steadily increases with the temperature,
92 from 0.3 to 0.8 (figure 2E). This increase in the fraction of turning bouts comes with an increase in their
93 associated reorientation angles $\delta\theta_{turn}$ as shown in figure 2H.

94 **The bath temperature controls the persistence time of the orientational state.**

95 In a recent study [19], we showed that the orientational dynamics of zebrafish larvae can be described by
96 two independent Markov chains (figure 3A). The first one controls the bout type selection, between forward
97 scoots or turn bouts. This process is essentially memoryless, such that the transition rates are simply set
98 by the ratio between either categories, namely p_{turn} and $1 - p_{turn}$. The second Markov chain controls the
99 orientations of the turning bouts. When a turn bout is executed and if this chain is in the left (right) state,
100 then the animal turns left (right, respectively). This second selection process has been shown to display a
101 persistence over a few bouts: the fish tends to chain turn bouts that are similarly orientated [19, 24–26].

102 Here we examined how this motor-persistence mechanism is impacted by the bath temperature. We estimated
103 the flipping rate p_{flip} - the probability to switch orientation at each bout - by first binning the turning
104 angles into three categories (denoted Δ) and assigning a discrete value to each of them: right turn ($\Delta = -1$),
105 forward bout ($\Delta = 0$) and left turn ($\Delta = +1$). We then computed the mean discretized angle value $\langle\Delta_{n+1}\rangle$ at
106 bout $n + 1$ for the three possible values of the previous bout Δ_n , as shown in figure 3B. The slope of the linear
107 fit provides a measurement of p_{flip} (see Methods and equation 1). This flipping probability increases with
108 temperature from 0.22 at 18°C to 0.45 at 33°C (figure 3C), approaching 0.5. Hence, at high temperatures,
109 the orientational persistence essentially vanishes, *i.e.* the probability to trigger a left *vs* a right turn becomes
110 independent of the orientation of the previous bout.

111 This approach yields a typical number of bouts $1/p_{flip}$ over which the turning orientation is maintained. A
112 complementary approach consists in characterizing the actual time-persistence (in seconds) of the orientational
113 state [19]. To do so, we assume that the orientation selection is driven by a hidden two-state continuous signal,
114 of which the turn bouts provide a stochastic sampling. We hypothesize that a forward bout is “transparent”,
115 *i.e.* it does not interfere with the persistence process, and that the orientational state remains unchanged
116 until a bout in the opposite direction is executed. The procedure for reconstructing the orientational signal is
117 illustrated in figure 3D.

118 For all trajectories, we computed the autocorrelation function (ACF, $R_{\Delta\Delta}$) of the reconstructed orientational
119 signals, and averaged them for each temperature (figure 3E). The ACF shows a faster decay for higher
120 temperatures, *i.e.* the time period over which the animal can maintain its orientational state is larger in
121 colder water. The ACFs could be correctly adjusted with an exponential decay, a functional form that is
122 expected for a simple telegraph process [27]. This suggests that the left/right transition over a time interval dt
123 is simply given by $k_{flip}dt$, where k_{flip} is the transition rate from one state to another. From the exponential
124 fit of the ACFs, we extracted k_{flip} , which we found to increase quasi-linearly with the temperature, as shown
125 in figure 3F (purple line). The rate k_{flip} is the temporal counterpart of the per-bout flipping rate p_{flip} , the

126 two quantities being linked through the interbout interval. Consistently, we found that $p_{flip}/\langle\delta t\rangle$ provides a
127 good approximation of k_{flip} for all temperatures (figure 3F, red line).

128 **Navigational kinematic parameters are statistically coupled.**

129 In the preceding sections, we showed that the bath temperature impacts in a systematic way the statistical
130 distributions of the five kinematic parameters that control the fish spontaneous navigation, namely the
131 interbout interval (IBI), turn amplitude, travelled distance, turn probability and orientational flipping rate.
132 When examining trajectories recorded at a given temperature, we noticed that they tend to fall in stereotypical
133 categories reminiscent of those most often observed at various temperatures. Some trajectories are tortuous
134 with short IBI, akin to typical hot water trajectories, while other appear to be straighter with less frequent
135 bouts as generally observed in cold water (figure 4A and 1C). This is suggestive of the existence of a finite
136 kinematic repertoire accessible to the animals whose relative occurrence may be controlled by the bath
137 temperature.

138 To test this intuition, we first aimed at establishing the statistical constraints that could set this accessible
139 repertoire. We thus examined the pairwise covariance of the aforementioned kinematic parameters. At
140 short time scale (over one bout), we did not observe any significant correlation between the 3 parameters
141 that can be evaluated on a per-bout basis (IBI, reorientation angle and travelled distance, see figure S1A).
142 However, when performing the same analysis on per-trajectory averages, we observed a robust covariance of
143 the parameters. This is illustrated in figure 4B which shows the covariance matrices computed for all data
144 and for each temperature. The IBI appears to be strongly anti-correlated with the forward displacement
145 and the flipping rate. In contrast, besides IBI, all pairs of parameter tend to exhibit positive correlations.
146 Importantly, these statistical features are conserved across the entire temperature range.

147 **Temperature controls the distribution probability within a well-defined locomotor repertoire.**

148 We thought to evaluate how this intra-temperature covariance of the navigational parameters aligned
149 with the inter-temperature covariance. To do so, we used the temperature-averaged parameters to build a 5
150 temperatures by 5 parameters matrix from which we computed an inter-temperature Pearson correlation
151 matrix (figure S1B). The latter displays a comparable structure as the mean intra-temperature correlation
152 matrix 4B: as we have shown in the previous sections, all parameters increase with temperature, and are thus
153 positively correlated, except for the interbout interval which decreases with the temperature and is therefore
154 anti-correlated with the 4 other parameters.

155 Hence, intrinsic variability and temperature-induced behavioral changes both reflect a concerted modulation
156 of the kinematic parameters along a similar axis. This can be illustrated by representing individual trajectories
157 as points in a four dimensional parameter space (figure 4C). This representation shows that the accessible
158 locomotor space is a continuum organized along a major axis, and that the bath temperature favors a
159 particular region of this manifold. To confirm this claim, we performed a principal component analysis on
160 both the inter-temperature and intra-temperature data. For all temperatures, the first principal component
161 (PC) explains 28 to 45% of the intra-temperature variance (figure 4D), *i.e.* significantly more than expected
162 for independent parameters (20%). Due to the small size of the inter-temperature matrix (5 samples), the

163 first PC explains more than 90% of the inter-temperature variance (figure S1C). The first PC is conserved
164 across the temperature range (figure 4E, colored bars) and essentially aligned with the inter-temperature PC
165 (black squares). The second PC is similarly conserved across temperatures (figure 4F) yet less clearly aligned
166 with its inter-temperature counterpart.

167 In order to represent data from various temperatures within the same low-dimensional space, we performed a
168 PCA analysis on the pooled covariance matrix, combining all intra-temperature arrays after standardization
169 (figure 4D-F, solid gray line). Based on the Guttman-Kaiser criterion, we only retained the first two principal
170 components [28] (figure S1D). Figure 4G shows the entire dataset projected in this unique 2D PCA space,
171 where the temperature is color-coded. As the temperature is increased, the accessible locomotor space is
172 shifted towards higher values of both marginal projections, with a concurrent widening of the distribution
173 for the first PC. These observations are thus in line with the view that the trajectories are confined to a
174 manifold defined by the correlation between the various parameters. Each temperature delimits a specific
175 accessible region of this subspace as defined by the PCs projection values.

176 **Single-fish recordings reveal a slow diffusive-like modulation of the locomotor behavior.**

177 The experiments on which these analysis were performed are based on simultaneous recordings of 10 fish
178 for each batch. As we can not track individual fish over the entire session, we can not evaluate to what extent
179 individual animals' navigational pattern may vary during the course of the assay. To address this specific
180 question, we performed a second series of experiments in which single animals ($N = 18$) were continuously
181 monitored for 2h at an intermediate bath temperature of 26°C. The same analysis pipeline was implemented.
182 In particular, the recordings were split into successive “trajectories” corresponding to wall-to-wall sequences.
183 We observed that over the course of the assay, the trajectories tended to exhibit strongly distinct features as
184 illustrated in figure 5A, reflecting a significant intra-individual behavioral variability.

185 For each individual, we similarly computed a feature matrix containing, for all successive trajectories, the
186 mean interbout interval, reorientation angle of turn events, displacement, turning probability and flipping
187 rate. We then performed a PCA on each array. Both the explained variance (figure S2A) and the PCA
188 coefficients (figure 5B-C) were unchanged with respect to the multi-fish analysis (5B-C, gray line). This
189 indicates that the covariance structure in the locomotion pattern is similar at the intra and inter-individual
190 level.

191 We thus used the multi-fish PC space defined in the preceding section to represent the single-fish data. The
192 result for an example fish is shown in figure 5D where the successive trajectories are indicated as dots in
193 this two-dimensional PC space. This representation reveals a slow diffusive-like exploration of the locomotor
194 space over the course of the experiment, with a progressive transition from one type of trajectory (e.g. long
195 displacements, frequent bouts, frequent turns) to another (e.g. short displacements, longer inter-bout intervals
196 and fewer turns).

197 To quantify the time-scale of this itinerant exploration within the locomotor space, we computed the
198 autocorrelation function (ACF) of the projections on the two first PCA components (5E-F, black line). These
199 curves could be captured by an Ornstein–Uhlenbeck (O.U.) process, which describes the dynamics of a

200 random walker within a quadratic energy basin [29, 30], see Methods). The latter allows one to bound the
201 stochastic exploration within a finite region of the locomotor space. From the fit, we extracted the times
202 needed for the dynamical system to reach its stationary regime: $\tau = 2585 \pm 58$ s for PC1, $\tau = 1980 \pm 14$ s for
203 PC2 (mean \pm s.e.m.). These values clearly demonstrate that the modulation of the exploratory behavior
204 in individual animals takes place over time scales that are orders of magnitude longer than the interbout
205 interval.

206 This series of experiments allowed us to further assess the relative contribution of the intra- and inter-individual
207 components in the observed behavioral variability. As the assay is longer (2h) than the time needed to reach
208 the stationary regime (~ 2000 s), each recording provides an estimate of the intra-individual variability. The
209 latter was quantified in the PC space as the variance of the PC projections across the entire duration of
210 the assay, averaged over the the various individuals. We then separately computed the variance of the PC
211 projections, pooling the data of all animals (figure S2D, green). The latter quantity thus encompasses both
212 inter- and intra-individual variability. This analysis led to the conclusion that a dominant fraction of the
213 variance (68% on PC1, 53% on PC2) can be explained by the intra-individual variability.

214 **Simulations of spontaneous navigation at various temperatures reveal basic thermophobic be-** 215 **havior without direct gradient-sensing mechanism.**

216 Having thoroughly characterized the statistical structure of the kinematic parameters and their thermal
217 modulation, we sought to build a minimal stochastic model of the fish navigation in order to generate synthetic
218 trajectories at different temperatures. Each kinematic parameter defines a random variable whose mean is set
219 by the temperature and whose statistical distribution accounts for both the inter-trajectory variability and
220 the per-bout stochasticity. The dual nature of the variability was mathematically recapitulated by expressing
221 each of the 5 kinematic variables as a product of two stochastic, temperature-independent variables: one
222 accounting for the trajectory-to-trajectory modulation (within a range controlled by the bath temperature,
223 figure S3B-E, Y column), and the other reflecting the remaining short-term variability (bout-to-bout, figure
224 S3B-E, ϵ column, see Methods). For the former, we used the copula method to reproduce the observed
225 covariance of the per-trajectory means of the various parameters.

226 This approach allowed us to generate various trajectories at different temperatures, as illustrated in figure
227 6A. These trajectories are qualitatively similar to those typically observed at the corresponding temperatures
228 (see figure 1C for a comparison). To quantify how this stochastic model captures the exploratory behavior,
229 we computed the mean square displacement (MSD, figure 6B) and the mean square reorientation (MSR,
230 figure 6C) on both the real (dots) and numerical data (solid lines). Overall, the exploratory dynamics appear
231 to be correctly reproduced by the numerical model. Importantly, the inter-trajectory variability is also, by
232 construction, correctly reproduced by this minimal model.

233 This model was used to probe how the temperature dependence of the navigational kinematics may participate
234 in driving the animal along thermal gradients. We first experimentally quantified how zebrafish larvae
235 responded to a linear thermal gradient spanning our temperature range (18°C-33°C), by focusing on the
236 steady-state occupation distribution. We found that the larvae favor regions where the temperature is
237 comprised between 23°C and 29°C (figure S4), *i.e.* they tend to avoid both extreme (hot and cold) regions.

238 The underlying sensory-motor mechanism is bound to involve both the effect of the temperature on the fish
239 navigation pattern (thermokinesis) and a direct (immediate) response to perceived temperature changes
240 (thermotaxis) [15, 17]. Our model allows us to assess the relative contribution of the kinesis process. In order
241 to do so, we implemented a simulation in which a virtual fish navigates in a rectangular pool ($L \times 45\text{mm}$) in
242 which we imposed a linear thermal gradient along the horizontal x -axis spanning the 18°C - 33°C range. We
243 simulated trajectories of numerical swimmers by continuously updating their exploratory statistics according
244 to the local bath temperature. These changes are entirely controlled by the temperature-dependence of the 5
245 kinematic parameters, which we linearly interpolated across the thermal gradient. Four gradient strengths
246 were emulated by changing the length L of the pool ($L = 0.1, 0.3, 0.5, 1\text{m}$).

247 The time evolution of the position distribution along the gradient are shown as heatmaps in figure 6D. They
248 reveal a global drift of the population towards the low temperature region for all values of the thermal
249 gradient (figure 6E). In all conditions, the distributions were found to converge towards a unique steady-state
250 profile after a finite time. The probability of presence in the steady-state regime displays a quasi-linear decay
251 from 18 to 26°C , and remains uniform at higher temperature. The thermokinesis process thus endows the
252 animal with a basic thermophobic behavior, even for minute gradients - orders of magnitude smaller than
253 those imposed in thermotactic assays. In contrast, the avoidance of cold regions seen in experiments (figure
254 S4, see Methods) is absent in our simulations, and must therefore reflect a direct gradient-sensing mechanism.

255 The dynamic of this thermophobic behavior in the simulations appears to depend on the imposed gradient, as
256 illustrated in figure 6F, which shows the mean experienced temperature across the population as a function
257 of time for the three gradients. All the curves display a similar decay associated with a global drift towards
258 the cold region, until a similar plateau value is reached, albeit with different time-scales. Due to the diffusive
259 nature of the fish spatial exploration, the settling time is expected to scale with the square of the pool length.
260 Consistently, the four dynamic evolution are found to fall on a unique curve when plotted as a function of
261 t/L^2 (figure 6G). The associated settling times range from 10 minutes for the largest gradient up to ~ 14
262 hours for the smallest one.

263 3 Discussion

264 Animal behaviors unfold as trajectories in a high dimensional space of motor actions. To make behavior
265 mathematically tractable, one needs to unveil statistical rules that couple the different components of the
266 behavior and organize them across time-scales. This dimensionality reduction approach is a pre-requisite to
267 further distinguish between deterministic and stochastic components of the behavior and concurrently discover
268 the underlying neural mechanisms [31, 32]. Leveraging novel techniques for high-throughput behavioral
269 monitoring and automatic classifications has allowed to elucidate the statistical structure organizing self-
270 generated behaviors in numerous species, such as *C. elegans* [33], *Drosophila* [34, 35], zebrafish [3, 22], or
271 mice [36].

272 With its bout-based navigation, zebrafish larva offers a relatively simple model for such an endeavour. It
273 has been shown that as few as 13 different swim bout types are sufficient to capture the entirety of its
274 behavioral repertoire [22]. Here we focus on spontaneous exploration in the absence of time-varying sensory

MARCH 17, 2021

275 cues. Within this limited scope, we were able to show that the knowledge of only 5 kinematic variables suffices
276 to characterize the long-term exploratory process. Indeed, synthetic trajectories generated by stochastic
277 sampling from the statistical distributions extracted from the data accurately reproduce the experimentally
278 observed angular and translational dynamics.

279 Using this reductionist approach, we were able to demonstrate that the variability in the fish exploratory
280 dynamics originates from two separate mechanisms, acting on distinct time-scales. Over a few bouts, the
281 fish displacement is akin to a random walk in which multiple stochastic processes set the successive values
282 of two discrete (bout type and turn bout orientation) and three continuous (Inter-bout-interval, linear and
283 angular displacements) variables that together define its instantaneous in-plane velocity. These processes
284 are statistically constrained by mean transition rates and amplitude probability distributions that can be
285 considered invariant at the scale of individual trajectories (*i.e.* over tens of bouts). These parameters however
286 vary significantly over long time scales: their time modulation takes place over hundreds to thousands of
287 bouts, indicative of a clear time-separation between the two different processes. Importantly, although we did
288 not observe any significant correlation in the instantaneous locomotor variables, the slow modulation of the
289 kinematic parameters exhibits robust covariance, and is thus constrained within a well-defined kinematic
290 manifold.

291 The present study allowed us to quantify how the water temperature modulates the locomotor statistics
292 of zebrafish larvae. Rather than evoking distinct locomotor patterns, temperature controls the relative
293 occupancy within this subspace: changing the temperature consistently impacts the mean value of the
294 kinematic parameters but leaves their covariance structure unchanged. Temperature thus essentially sets the
295 accessible range of exploratory trajectories within a well-defined continuum of possible locomotor behaviors.

296 At the circuit level, it is tempting to interpret these observations by considering the brain as a dynamical
297 system exhibiting multiple metastable patterns of activity (brain states) whose relative stability and transition
298 rates define a particular energy landscape [37]. In this view, the short-time dynamics that select the successive
299 bout properties correspond to a stochastic itinerant exploration of this neuronal landscape. The latter is
300 essentially invariant over minutes but is slowly reshaped via endogenous processes or through temperature
301 changes, leading to a gradual modification of the short-term statistics. In a concurrent study (unpublished),
302 we directly tested this hypothesis by focusing on the selection of turn bout orientation, a process whose
303 neuronal substrate is known. The ARTR (anterior rhombencephalic turning region), a small bilaterally
304 distributed circuit, has indeed been shown to control the selection between left and right turns. This circuit
305 displays an endogenous antiphase alternation between the left and right subcircuits. Turn bout orientation is
306 systematically ipsiversive to the active population at the time that they are executed [25, 26]. In this study,
307 we report an increase in the frequency of the ARTR endogenous oscillation with the temperature in line
308 with our present behavioral observations. Using Ising models, inferred from the ARTR dynamics recorded
309 at various temperatures, we were able to unveil how the ARTR energy landscape is indeed reshaped as the
310 temperature is increased such as to favor more frequent transitions between the left and right states.

311 Slow modulation of locomotor characteristics in zebrafish larvae have been reported in two recent studies
312 [2, 3]. In [2], the authors identified two discrete states, associated with exploration and exploitation during

MARCH 17, 2021

313 foraging, with typical persistent times of order of minutes. In [3], progressive changes in locomotor statistics
314 were associated with decaying hunger state, as the initially starved animal progressively reached satiety. In
315 contrast with these two studies, the modulation in locomotor kinematics that we observed is continuous and
316 does not reflect spatial heterogeneities in the environment (e.g. local presence of preys) or explicit changes in
317 internal states such as satiety. With respect to hunger state, the use of temperature may offer a practical way
318 to externally drive the internal state to a stationary point in an ethologically relevant way.

319 The neuronal basis of this internal state modulation process remains to be elucidated. The circuits regulating
320 specific locomotor features, such as the bout frequency [38] or orientational persistence [25, 26] have been
321 identified. However, the fact that the various kinematic parameters display concerted endogenous modulations
322 points towards a global drive. Temperature is known to impact cellular and synaptic mechanisms [39] in
323 such a way that an increase in temperature tends to speed up neuronal oscillatory processes [40, 41]. This
324 may explain the concurrent decrease in the persistent times associated with the orientational persistence and
325 interbout intervals. The thermal modulation of the angular and linear amplitude of the bouts may in turn
326 reflect a temperature dependence of the muscular efficiency rather than neuronal processes [42]. Another
327 possibility is that the temperature drives the activity level of neuromodulatory centers which may also exhibit
328 slow endogeneous modulations. This neuromodulation release would then globally impact the spontaneous
329 dynamics of various premotor centers yielding the observed change in locomotor patterns. The serotonergic
330 neurons of the dorsal raphe constitute an attractive candidate for such a mechanism as their activation has
331 been shown in numerous instances to drive a persistent change in behavior in zebrafish [2, 6, 43], as well as in
332 mice [44].

333 Our study yields a minimal numerical model of zebrafish locomotion at different temperatures. This model
334 allowed us to probe *in silico* how the thermal modulation of the exploratory dynamics may contribute to the
335 thermotaxis behavior, thus complementing direct gradient-sensing mechanisms [18]. Our simulations indicate
336 that this thermokinesis process endows the animal with the capacity to efficiently avoid hotter regions, but
337 cannot explain the observed avoidance of cold water. As thermal gradient sensing operates within a time
338 window of 400ms [17], it may be ineffective in conditions where the lengthscale of thermal gradients is much
339 larger than the typical distance travelled per bout. In such conditions, this complementary mechanism may
340 be strategically relevant as it allows the animal to navigate away from potentially noxious regions.

341 This study establishes the temperature as an effective and practical external parameter to explore behavior
342 variability in vertebrates. Our analysis provides simple latent variables, namely the two first PCA projections,
343 that can be used to efficiently track the animal's behavioral state. Changes in behavioral states are generally
344 induced through complex protocols, involving a perturbation of a sensorimotor loop, or through abrupt
345 changes in sensory conditions [45]. In such approaches, the change is discrete and generally transient as the
346 animal eventually adapts to the new conditions. In contrast, temperature offers a way to drive a robust,
347 continuous and chronic shift in behavior that can be easily implemented while performing large-scale brain
348 monitoring. Various behavioral states are thought to reflect different levels of attention or arousal, which
349 in turn impact the responses to sensory stimulation. Beyond its utility for studying how a given neuronal

MARCH 17, 2021

350 circuit may give rise to distinct dynamics, as illustrated in [46], thermal perturbation could also be leveraged
351 to investigate how internal states may enhance or inhibit sensory responses.

352 **Acknowledgements**

353 We thank the IBPS fish facility staff for the fish maintenance, in particular Stéphane Tronche and Alex Bois.
354 We are grateful to Carounagarane Dore for his contribution to the design of the experimental setup, Geoffrey
355 Migault for engineering expertise and Raphaël Voituriez for fruitful discussion on the modeling aspects. This
356 work was funded by the CNRS, Sorbonne Université and the Systems Biology Network of Sorbonne Université
357 and supported in part by the Human Frontier Science Program under grant No. RGP0060/2017, by the
358 french Research National Agency under grant No. ANR-16-CE16-0017 and the European Research Council
359 under the European Union's Horizon 2020 research and innovation program grant agreement No. 715980.

360 **Authors contribution**

361 G.L.G., R.C. and R.C. conceived the project. R.C. designed the setup. G.L.G. performed the experiments.
362 G.L.G., S.K. and G.D. analyzed the data. All authors contributed to the manuscript.

363 **Declaration of interests**

364 The authors declare no competing interests.

MARCH 17, 2021

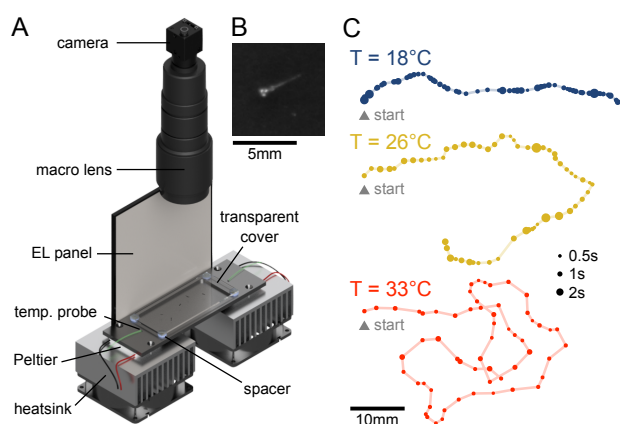


Figure 1: Behavioral assay for the video-monitoring of spontaneous navigation of zebrafish larvae at different temperatures. **A** Sketch view of the setup: Larval zebrafish are freely swimming in a rectangular pool connected to a pair of Peltier modules in a light-tight box. The setup is illuminated with a white electroluminescent (EL) panel and a symmetrically positioned a mirror (not shown). The tank is covered with a transparent slide to limit evaporation. A CMOS camera records images at 25 frames per second. **B** Blow-up of a raw image around a larva. **C** Example trajectories extracted offline from movies recorded at different temperatures. Each dot represents a bout event, with size encoding the time spent at this location.

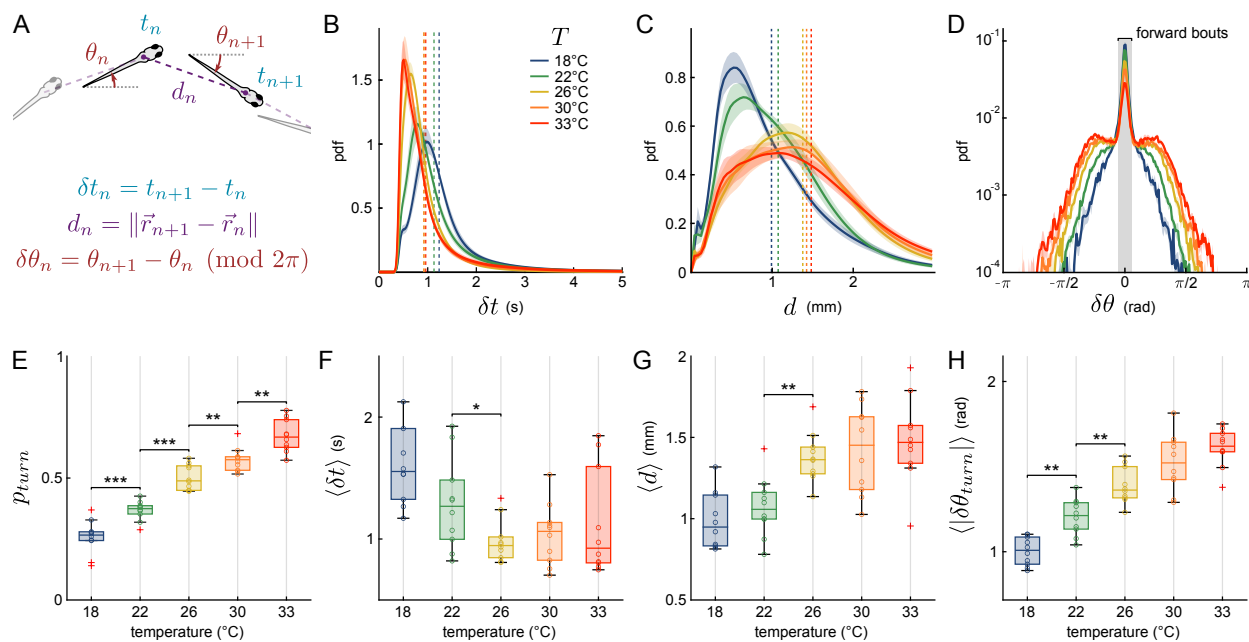


Figure 2: Effects of bath temperature on spontaneous navigation. **A** Sketch defining three kinematic parameters. δt_n is the time elapsed between bout n and bout $n + 1$, known as the interbout interval. The displacement d_n is the distance travelled during bout n (in mm), while $\delta \theta_n$ represents the reorientation angle. A small value around 0 corresponds essentially to a forward swim, while a large positive value (resp. negative) corresponds to a left (resp. right) turn. **B-D** Per-batch averaged distributions of interbout intervals (**B**), displacements (**C**) and turn angles (**D**) for each tested temperatures. Vertical dotted lines are the means of the distributions, shaded areas are standard errors of the mean (sem). The gray area in **D** marks the forward events versus the turn events. **E-H** Boxplots of selected parameters. Each dot corresponds to a batch of 10 fish, the box spans the 25th to the 75th percentiles, the horizontal line is the median, red crosses are outliers. Significance given only for neighboring boxes (Kruskal-Wallis test, no star : $p > 0.05$, * : $p < 0.05$, ** : $p < 0.01$, *** : $p < 0.001$). **E** Fraction of turns, referred to as the turning probability, defined as the ratio of turn bouts over the total number of bouts. **F** Means of the interbout intervals. **G** Means of the displacements. **H** Means of the absolute reorientation amplitude of turning bouts.

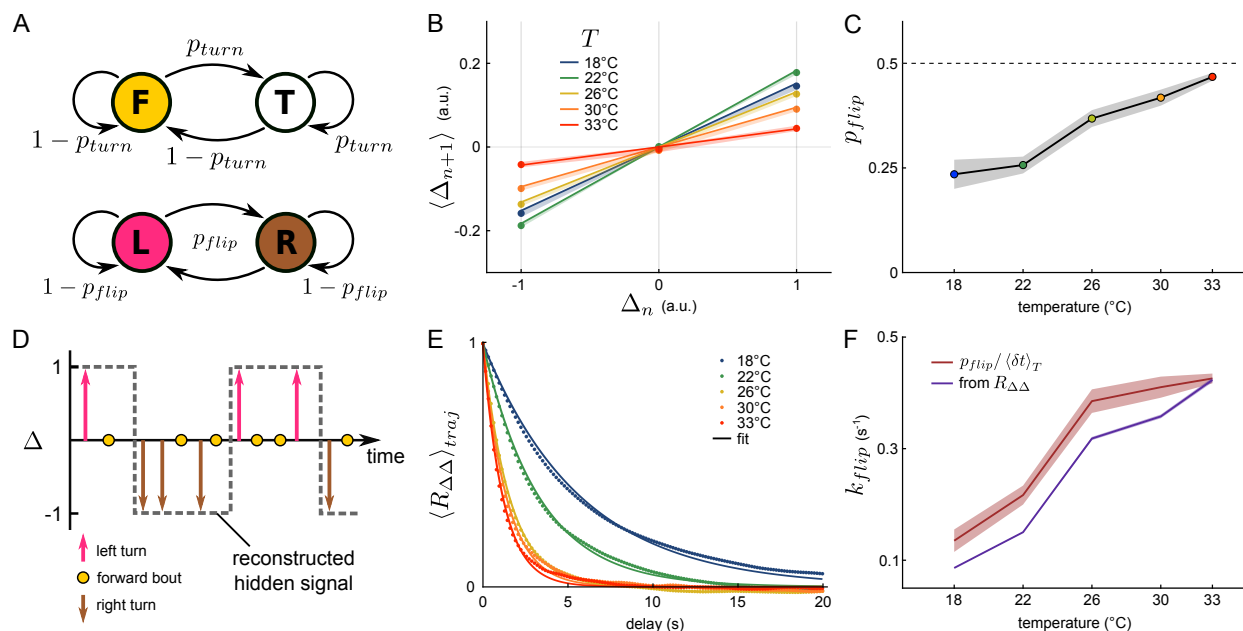


Figure 3: The orientational dynamics is temperature-dependent. **A** Two discrete and independent Markov chains describe the reorientation dynamics. The first one (top) selects the bout type, either turn (T) or forward (F), given the transition rate p_{turn} , while the second one (bottom) determines if the fish is in the left (L) or right (R) state with a transition rate denoted p_{flip} . **B** Mean ternarized reorientation Δ of the next bout, given the current bout reorientation. Shaded area is the sem, solid line is the fit (equation 1). **C** Temperature dependence of p_{flip} . The dashed line at 0.5 indicates a memoryless process. **D** Schematic representing a motion sequence generated by the two discrete Markov chains. The hidden underlying orientational signal that sets the left/right state of the fish is exposed only when the fish performs a turning bout and can be estimated (dashed line) for each trajectory. **E** Trajectory-averaged autocorrelation function of Δ ($R_{\Delta\Delta}$) and associated fit (equation 2). **F** Temperature dependence of k_{flip} , extracted from two methods: p_{flip} divided by the mean interbout interval associated with each temperature (red, shaded area is the s.e.m.) and from the fit of the autocorrelation function (purple, error bar 95% confidence interval).

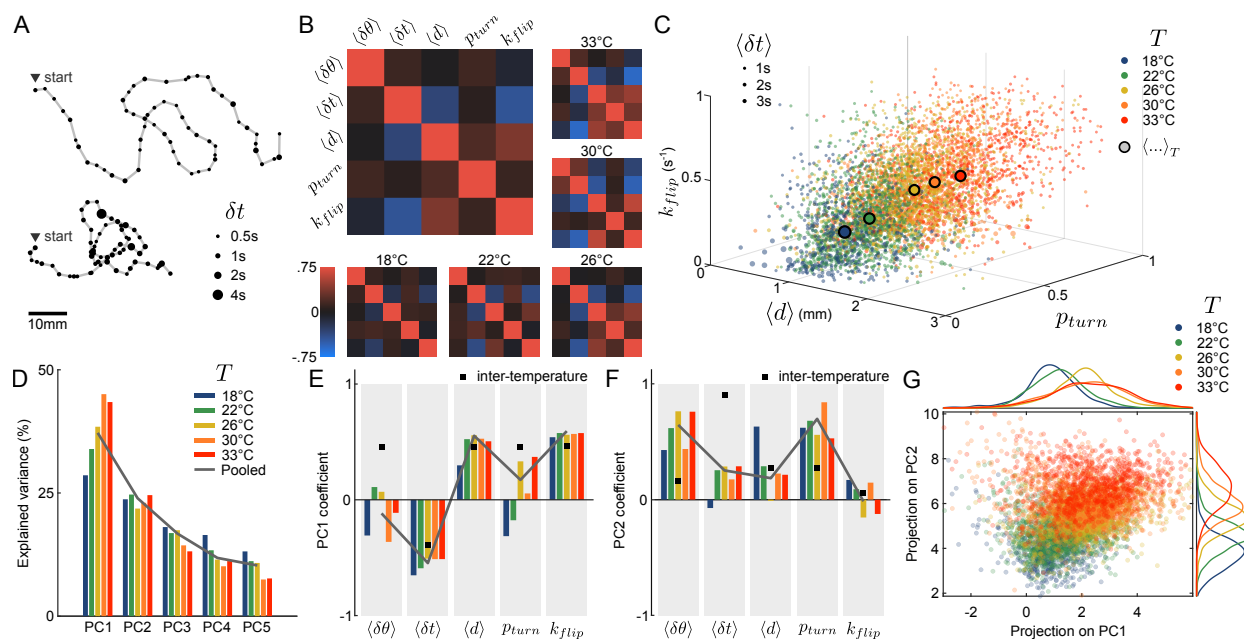


Figure 4: Correlations between parameters are conserved across temperatures. **A** Two qualitatively different trajectories recorded at the same temperature (30°C). **B** Pearson’s correlation matrices of the average reorientation angle $\delta\theta$, interbout interval δt and displacement d , along with the turning rate k_{turn} and flipping rate k_{flip} defined for each trajectory, at different temperatures. Large panel: average over all temperatures. **C** All per-trajectories values in the 4-dimensional parameter space of correlated variables. Dot size encodes interbout intervals, large black-circled dots are temperature-averaged parameters with IBI not encoded. **D** Variance explained by each principal component of a PCA performed on each intra-temperature feature matrix. **E-F** Coefficients of the principal components for intra-temperature matrices (colors), for the inter-temperature averaged matrix (black square) and for the pooled per-temperature array (solid line). **E** First principal component (PC1), **F** second principal component (PC2). **G** All per-trajectory values projected into the principal component space (first two PCs), and their associated marginal distributions for each principal vector.

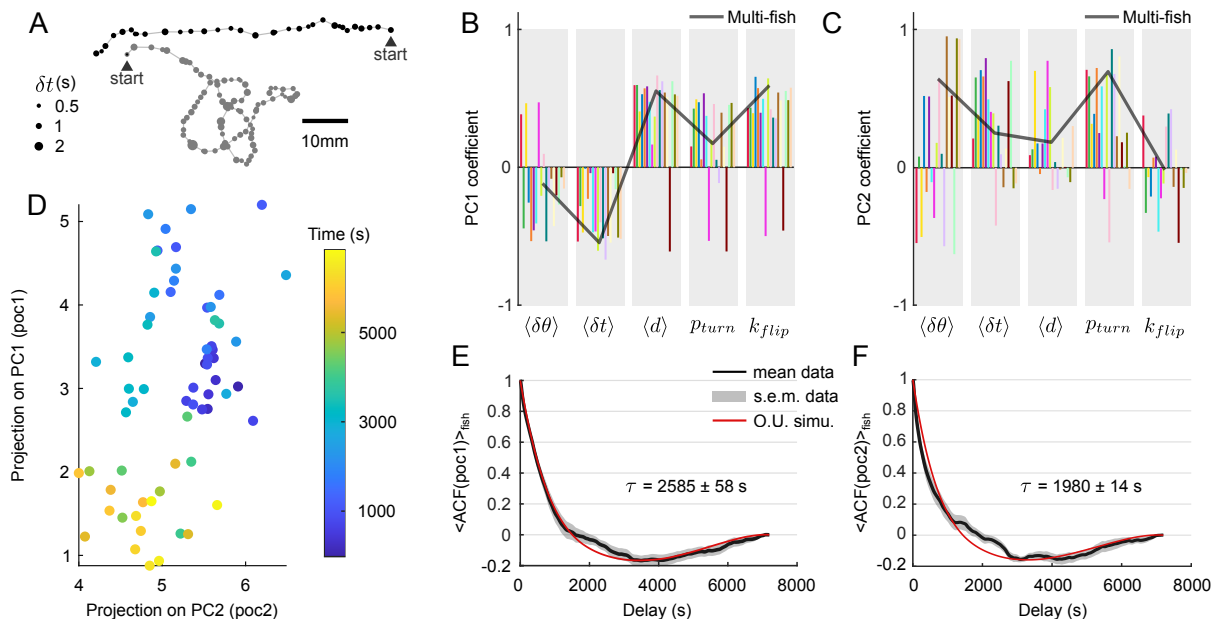


Figure 5: Diffusive-like exploration of the behavioral manifold for individual fish. **A** Two qualitatively different trajectories from the same fish at the same temperature (26°C), recorded at 1h interval. **B-C** Coefficients of the two first principal components for 18 different fish (one color corresponds to one fish). The solid line is the PC coefficients computed from the multi-fish experiments as shown in figure 4E-F. **D** Time-evolution of the projections in the 2D PCA space from an example fish. One dot corresponds to one trajectory whose parameters are projected on the multi-fish PC space. Color encodes the time at which the trajectory starts. **E-F** Autocorrelation function of the projections on **(E)** PC1 and **(F)** PC2, averaged across fish. Gray area is the standard error of the mean. Red line is the autocorrelation function of a simulated Ornstein-Uhlenbeck process whose bias parameter ($1/\tau$) is fitted to the data.

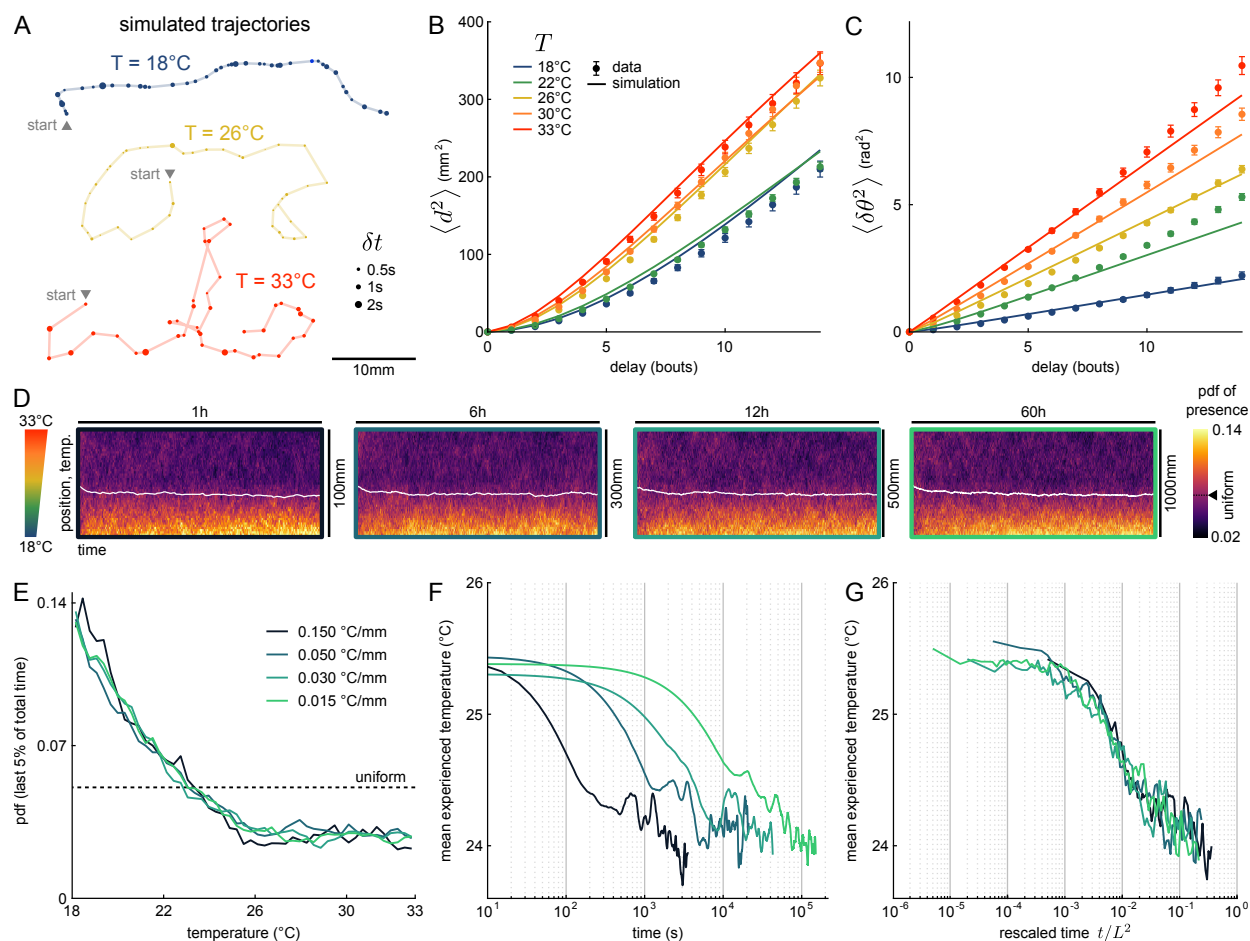


Figure 6: Simulations indicate that zebrafish does not need gradient information to perform negative thermotaxis. **A** Example trajectories generated with a simulation based on rescaled multivariate distributions (see Methods). **B** Mean square displacement, from data (dots) and simulation (line). **C** Mean square reorientation, from data (dots) and simulation (line). **D** Distributions of presence of simulated fish through time, for four strengths of temperature gradient. The white curve is the average position over time. The expected value for a uniform distribution is highlighted on the colormap. **E** Steady-state distribution of presence as a function of temperature. The dashed line is the expected value for an uniform distribution. **F** Temporal evolution of the average position over time (only the first 75 bins are shown for readability). **G** Distribution mean as a function of the time rescaled by the squared pool length.

365 4 STAR Methods

366 **Animals maintenance** Experiments were performed with wild type *Danio rerio*, aged 5 to 7 days post-
367 fertilization (dpf). Larvae were reared in Petri dishes containing embryo medium (E3), at 28°C, with a 14/10
368 hours cycle of light/dark and were fed with nursery powder GM75 everyday from 6dpf. Experiments were
369 done during daytime, in E3. They were approved by Le Comité d'Éthique pour l'Expérimentation Animale
370 Charles Darwin C2EA-05 (02601.01).

371 **Experimental setup** A pool made of copper ($100 \times 45 \times 2.5$ mm³) painted in black (Rust-Oleum) is stuck
372 on two 78W Peltier modules (Adaptive) with thermal tape (3M). A transparent, 2mm-thick PMMA cover is
373 placed over the pool with 2mm spacers to minimize water evaporation, leaving a water thickness of 4.5mm.
374 To check the harmlessness of this confined configuration, ten zebrafish larvae were left overnight inside
375 the setup. All survived and were swimming actively. The temperature is measured at both ends of the
376 pool with thermocouples type T (Omega). The two left/right error signals ($T_{target} - T_{measured}$) are used
377 within two independent PID loops implemented on an Arduino Uno board (Arduino) whose coefficients
378 have been optimized manually. Each PID regulates the PWM frequency sent to a H-bridge driving the
379 power sent to the two Peltier modules. A graphical user interface (GUI) written in C++ using the Qt
380 framework is used to monitor the measured temperatures and to impose the target temperatures on both
381 ends. Due to its high thermal diffusivity, the copper piece quickly reaches a uniform temperature and acts as
382 a thermostat for the water. After about 4 minutes, the temperature of the water in the center of the pool
383 has reached the set temperature ($\pm 0.2^\circ\text{C}$), which then remains constant over time. The GUI monitors the
384 bath temperatures while grabbing frames from a CMOS camera (FLIR Chameleon3 CM3-U3-13Y3M-CS)
385 coupled with a macrolens (Navitar) at 25 frames per second. The whole apparatus is placed in a light-tight
386 box, illuminated with a homogeneous white light emitted by a LED panel (Moritex) placed on the side; a
387 mirror placed at the other side limits significant phototactic bias in the small direction of the pool. All codes
388 mentioned above are available on Github (<https://github.com/LJPZebra/ThermoMaster>) under a GNU
389 GPLv3 licence. Blueprints of the box and pool as well as electronic designs are available upon request.

390 **Experimental protocols** The pool is filled with E3. A temperature is randomly drawn from 18, 22, 26,
391 30, 33°C and set with the GUI. After 10 minutes, a batch of 10 zebrafish larvae is introduced in the pool.
392 After 10 minutes of habituation, the fish kinematics are monitored for 1800s (half an hour). We checked for
393 steady-state by looking at mean presence distributions and mean bout frequency distributions during three
394 time windows (beginning, middle and end of the 1800s). The distributions within each time-window are not
395 significantly different ($p > 0.1$, two-sample Kolmogorov-Smirnov test). Fish remain in the pool while we
396 randomly draw a new non-tested temperature. After 20 minutes (temperature regulation and habituation), a
397 new recording of 1800s is performed. The five temperatures are not systematically tested on all batches, but
398 for each temperature, 10 different batches of 10 fish are used. In total, the experiments involved 17 different
399 batches. The sample size was not statistically determined beforehand.

400 For single-fish experiments, the same protocol is used except that a single fish was placed in the pool. The
401 recordings last for 2h and only $T=26^\circ\text{C}$ is tested.

402 For thermal gradient experiments (figure S4), 10 larvae are used during 45 minutes. The first 5 minutes are
403 recorded with a uniform temperature of 22°C, then a linear gradient is imposed during 40 minutes, from 18°C
404 to 33°C. The gradient direction (*i.e.* which side is set to either 18°C or 33°C) is chosen randomly. 10 different
405 batches are tested. The distribution of presence along the gradient is computed over the last 2 minutes (5%
406 of the gradient duration) such as to allow enough time for the animals to reach a steady-state.

407 **Tracking and basic analysis** Larvae were tracked offline using the open-source FastTrack software [23],
408 <https://www.fasttrack.sh>). It generates a text file containing the position of each fish's center of mass
409 and body angle across frames until they leave the defined ROI. Kinematic analyses were performed using
410 MATLAB (R2020a, Mathworks). Bouts are detected when the instantaneous speed is greater than two times
411 the overall variance of the speed. Putative bouts are then filtered on a distance criterion (bouts with a
412 linear displacement - measured in a time window of $\pm 0.5s$ centered on the bout onset - less than 0.3mm
413 or greater than 18mm are rejected) and on a temporal criterion (bouts occurring within 0.4s after a bout
414 are rejected). Bout timing is defined as 80ms before the velocity peak. Detection performance was checked
415 manually on randomly selected sequences. From positions, time and body angles before and after a bout
416 event, we computed displacements, interbout intervals, and turn angles associated with each bout. Data are
417 split into trajectories, from one edge of the ROI (set at 5mm from the walls) to another. Only trajectories
418 that last at least 25 seconds, with at least 10 bouts, with 3 bout types (left turn, right turn and forward scoot)
419 are kept for further analysis. Trajectories last on average 67s (median 47s, 95th percentile 178s) and contain
420 on average 60 bouts (median 44 bouts, 95th percentile 154 bouts). All MATLAB routines are available on
421 Gitlab (<https://gitlab.com/GuillaumeLeGoc/thermomasterlab>) under the GNU GPLv3 licence.

422 **Bout classification** To discriminate whether a bout falls in the forward or the turning categories, we
423 fitted the one-sided (absolute value) reorientation angles distributions with the sum of a zero-mean Gaussian
424 distribution and a gamma distribution. The Gaussian corresponds to the part of the distribution close to zero,
425 while the gamma function aims at describing the distribution of high angles reorientations. We manually
426 set the Gaussian width and the scale parameter of the gamma function based on the observed distributions.
427 We fitted the shape parameter for each temperature, ensuring that the slope at high angles in logarithmic
428 scale is well reproduced. Then, we defined a fixed threshold for the angles to be considered as a turn or a
429 forward bout. This threshold is the angle at which the two distributions cross, invariably found around 10°
430 ($10.25 \pm 0.23^\circ$, mean \pm sd). This value of 10° (0.17rad) was used to classify bouts throughout this work.

431 **Displacement correction** We noticed that the displacement corresponding to a turn event was systemati-
432 cally larger than the displacement associated to a forward event. This is due to the fine structure of a turning
433 bout: first, the fish performs a small reorienting bout, then it scoots forward [21]. Since we do not look at
434 this fine structure, the overall displacement during a turn bout is geometrically overestimated and would bias
435 temperature-to-temperature comparison. We computed the ratio between displacements during turns and
436 the ones during forward swims, and found a factor of 1.6 ± 0.1 , regardless of the temperature. Therefore, in
437 all analyses presented in this work, all displacements corresponding to a turn event were corrected by a factor
438 $1/1.6 = 0.625$.

439 **Statistical methods** Probability density functions (pdf) were computed with a kernel density estimation
 440 through the built-in Matlab function `ksdensity`, with a bandwidth of 0.1 for interbout intervals and
 441 displacements and 0.5 for turn angles. For the distributions of figure 2, a pdf was computed for each batch
 442 and the mean and standard error of the mean are computed. For rescaled curves (figure S3), data from all
 443 experiments were pooled to compute the temperature-average quantity \overline{X}_T and rescaled values. Boxplots
 444 were made with the built-in Matlab function `boxchart`, using as input data the means of the respective
 445 quantities for trial (one dot corresponds to a batch of 10 fish). For simulations of navigation, averages over
 446 temperature were computed by pooling all bout events from all experiments corresponding to this particular
 447 temperature. p_{turn} and p_{flip} values were estimated for each trajectory and then averaged. Error bars for
 448 those temperature averages and for the pdf shown in figure S3 were all computed using bootstrapping with
 449 1000 boots to get the 95% confidence interval through the built-in `bootci` function. Errors were propagated
 450 for the ratio of p_{flip} and $\langle \delta t \rangle_T$ in figure 3F.

451 **Reorientation dynamics** The two Markov chains model has been described in details in a previous study
 452 [19]. We first binned the reorientation angles $\delta\theta$ into a ternarized reorientation Δ , with values -1 (right
 453 turn R), 0 (forward bout F) and +1 (left turn L). To extract p_{flip} , we analytically derived the mean
 454 reorientation Δ_{n+1} given the previous reorientation Δ_n . There are 9 combinations of bouts $\{n; n+1\}$:
 455 $\{L; L\}, \{L; R\}, \{L; F\}, \{F; L\}, \{F; R\}, \{F; F\}, \{R; L\}, \{R; R\}, \{R; F\}$. All combinations involving a forward
 456 bout yield 0. Remain combinations with two turns in the same direction and two turns in the opposite
 457 direction. For a turn in direction L (resp. R), the associated probability corresponds to the case where a flip
 458 occurred (*i.e.* the previous bout was in direction R , resp. L) and the case where no flip occurred (*i.e.* the
 459 previous bout was in direction L , resp. R). Noting Δ_n^R and Δ_n^L the turns in the right and left direction at
 460 bout n , the mean reorientation given the direction of the previous bout reads :

$$\begin{aligned}\langle \Delta_{n+1} \rangle_{\Delta_n^L} &= p_{turn}(p_{flip}\Delta_n^R + (1 - p_{flip})\Delta_n^L) \\ \langle \Delta_{n+1} \rangle_{\Delta_n^R} &= p_{turn}(p_{flip}\Delta_n^L + (1 - p_{flip})\Delta_n^R)\end{aligned}$$

461 These equations can be summed up as:

$$\langle \Delta_{n+1} \rangle_{\Delta_n} = p_{turn}(1 - 2p_{flip})\Delta_n \quad (1)$$

462 This is the fit used in figure 3B.

463 A random telegraph signal is a binary stochastic process with constant transition probability per unit of time.
 464 In the case where both states are equiprobable, the two transition rates (here noted k_{flip}) are equal. For
 465 such processes, the time spent in one or the other state (left or right) is exponentially distributed [27] and
 466 the autocorrelation function for a zero-mean signal reads :

$$R_{\Delta\Delta}(t) = e^{-2k_{flip}t} \quad (2)$$

467 This is the fit used in figure 3E.

468 Mean square displacement (MSD) $\langle d^2 \rangle$ and mean square reorientation (MSR) $\langle \delta\theta^2 \rangle$ were computed using
469 the MATLAB package `msdanalyzer` [47]. All (x, y) and $\delta\theta$ sequences are pooled by temperature for both
470 data and simulations, the MSD and MSR were computed for each sequence and we show in figure 6B-C the
471 ensemble average for each temperature with the standard error of the mean.

472 **Principal components analysis** The “features matrices” were built for each temperature. They include,
473 for each trajectory, mean interbout intervals, turn probability, flip rate (estimated as $p_{flip}/\langle \delta t \rangle$, p_{flip} being
474 extracted as explained above, for each trajectory), mean reorientation angle of turning events and mean
475 displacements. Each set was standardized (centered and normalized by its standard deviation) before being
476 processed by the single value decomposition (SVD) algorithm through the built-in `pca` function. Those 5
477 intra-temperature standardized arrays are then concatenated to form the so-called pooled matrix, that is in
478 turn used to find a common space through PCA. For projection, each set was normalized by the standard
479 deviation of all the pooled data (regardless of temperature) and not centered for comparison purposes. The
480 aforementioned common space was also used to project data from single-fish experiments.

481 **Numerical Ornstein–Uhlenbeck process** The single-fish experiments contains 48 ± 16 trajectories
482 (mean \pm s.d.). One trajectory translates to one point in the PC space, therefore we linearly interpolated the
483 projections in order to have PC projections defined on the same time vector that corresponds to the experiment
484 duration (7200s), sampled every second. For each fish, on both PC, we computed the autocorrelation function
485 (figure S2B-C) and averaged them (figure 5E-F, black line is the mean, shade is the s.e.m.).

Numerical simulations of the Ornstein–Uhlenbeck (O.U.) process were sequentially implemented using the following equation [48] :

$$X_{i+1} = X_i + \sqrt{2D}\mathcal{N}_i\sqrt{\delta t} + k(\mu - X_i)\delta t$$

486 where D is the diffusion coefficient (units $[X]^2.s^{-1}$), $k = 1/\tau$ the bias term (units s^{-1}), μ the drift term
487 (units $[X]$), δt the time interval chose for the simulation (units s) and \mathcal{N} is a random number drawn from a
488 normal distribution. In our case, the drift term was always 0.

489 To determine τ , we generated 500 realisations of the O.U. process with D set to 1 and τ set to values in a
490 given range. For each realisation, we computed the autocorrelation function (ACF) and averaged them across
491 realisations. We then computed the residual sum of square (RSS) and chose the minimum one to select the
492 best parameter τ . After manually narrowing down the best range for τ (PC1 : 2000s to 3000s, 1000 values;
493 PC2 : 1900 to 2100s, 1000 values), we repeated the previous process 20 times to get 20 “best τ ” and we
494 report the mean \pm s.e.m. in the text and figure.

495 **Numerical simulations of trajectories** Trajectories were simulated using the framework described in
496 figure S3, based on the hypothesis that (1) spatio-temporal dynamics can be reproduced solely from five
497 parameters, (2) per-bout values of interbout intervals (δt), displacements (d) and turn angles ($\delta\theta$) are drawn
498 from a distribution that can be decomposed as $X = \bar{X}_T Y \epsilon$, (3) the per-trajectory values of turning probability
499 (p_{turn}) and flipping probability (p_{flip}) are drawn from a distribution that can be decomposed as $X = \bar{X}_T Y$
500 and (4) the trajectory-averaged parameters are correlated. Note that for the simulations we use p_{flip} rather
501 than flipping rate for simplicity in the code implementation.

502 \bar{X}_T , the temperature average. All per-bout values of δt , d , reorientation angle of turn events ($\delta\theta_t$) and
503 reorientation angles of forward events ($\delta\theta_f$) are pooled by temperature and the mean is computed. A p_{turn}
504 and a p_{flip} is estimated for each trajectory, pooled by temperature and averaged (figure S3B-E, left column).

505 Y , the trajectory means variability. For each trajectory, a mean value is computed for δt , d and $\delta\theta_{t/f}$
506 while p_{turn} and p_{flip} are extracted. They are then rescaled by the corresponding temperature average value
507 computed above. For each temperature, a cumulative density function (cdf) is computed. They are then
508 averaged across temperatures to get a single Y cdf for each parameters (pdf shown in figure S3B-E, middle
509 column).

510 ϵ , the per-bout variability. Similarly, for each trajectory we rescale values of δt , d and $\delta\theta_{t/f}$ by their
511 corresponding trajectory mean. Then, all events are pooled by temperature and a cdf is computed. Finally,
512 we will use the mean cdf, resulting in a single ϵ cdf for per-bout parameters. p_{turn} and p_{flip} are defined for a
513 trajectory, hence they do not have bout to bout variability (pdf shown in figure S3B-D, right column).

514 *Correlations of means.* We compute the Pearson's correlation matrix of the trajectories' parameters (trajectory
515 means and probabilities), for each temperature. The coefficients are then averaged to get a single correlations
516 matrix $\langle R_{traj} \rangle_T$.

517 *Algorithm.* After choosing a number n of fish (trajectories), we generate multivariate distributions (copulas)
518 with the MATLAB built-in `mvnrnd` function, with the mean $\langle R_{traj} \rangle_T$ correlations matrix as input. It produces
519 5 marginal sets of n gaussian random numbers, correlated with one another. We then get the corresponding
520 normal cdf, which is in turn used to sample the corresponding Y cdfs, inverting the latter. Finally, those
521 samples are multiplied by the corresponding temperature average \bar{X}_T . A bout is generated by sampling
522 a displacement and a turning angle, along with a interbout interval during which the virtual fish stands
523 still, from the generic cdf of ϵ . Those values are multiplied by the trajectory means drawn earlier, and the
524 new position (x, y) is computed. The next bout is generated, and so on. For the gradient simulations, the
525 same strategy is used, at the notable difference that the temperature averages are determined dynamically
526 given the position of the agent along the temperature gradient. We used reflective boundary conditions. We
527 checked the consistency between parameters distributions from the data and from the simulations, as well as
528 correlations between trajectory means.

529 **Supplementary materials**

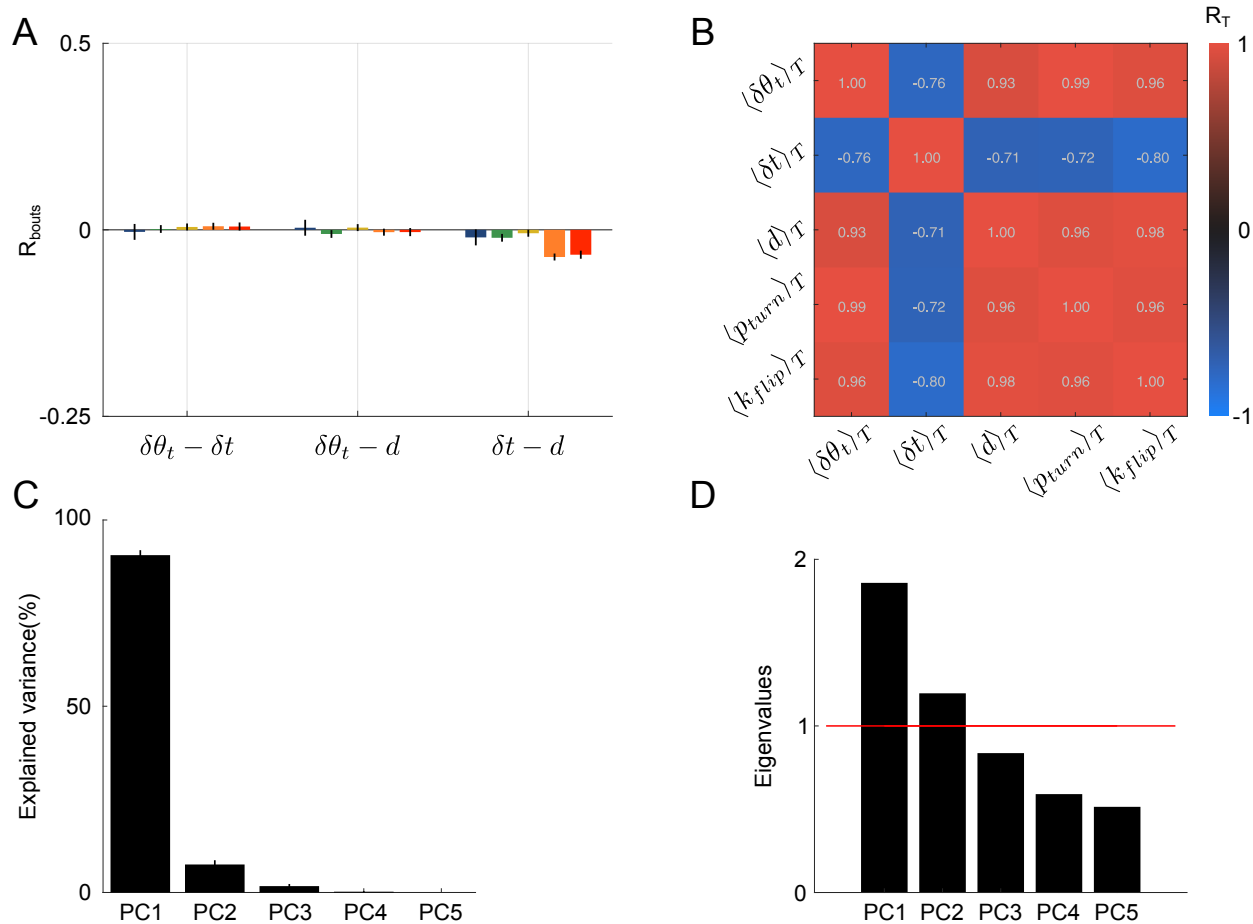


Figure S1: Correlations between parameters. **A** Pearson's correlation coefficients between per-bout parameters, reorientation angles of turn bouts, interbout interval and displacement. **B** Pearson's correlation matrix between temperature-averaged parameters. **C** Variance explained by the principal components of the inter-temperature matrix. **D** Eigenvalues of the pooled intra-temperature matrix. The red line highlights the Kaiser-Guttman criterion.

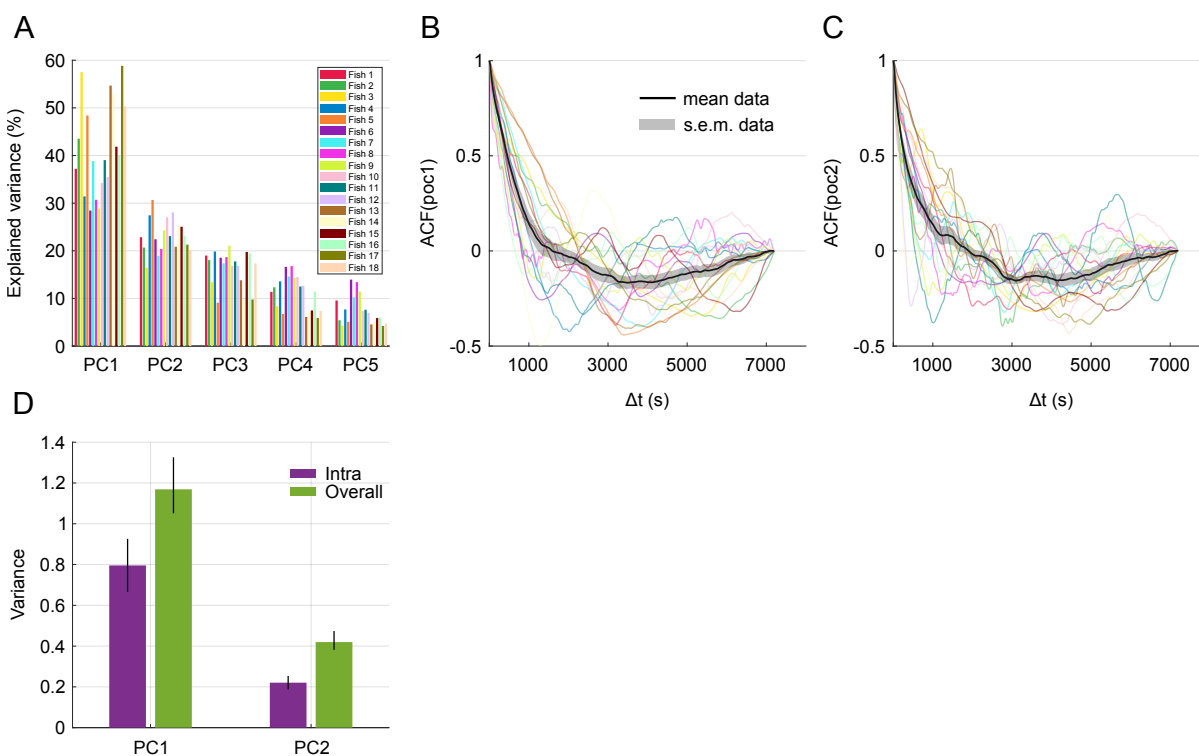


Figure S2: PCA in single-fish experiments. **A** Variance explained by the five principal components for each single-fish. **B-C** Autocorrelation function of the projection on PC1 (B) and PC2 (C) from each fish in single-fish experiments. The color code is the same as in A, black line and shaded area is the mean and s.e.m. across fish. **D** Mean variance of projections across time (intra, purple) and overall variance of projections (green). Error bars for intra is the s.e.m. and error bars for overall is 95% confidence intervals after bootstrapping (n=1000 boots).

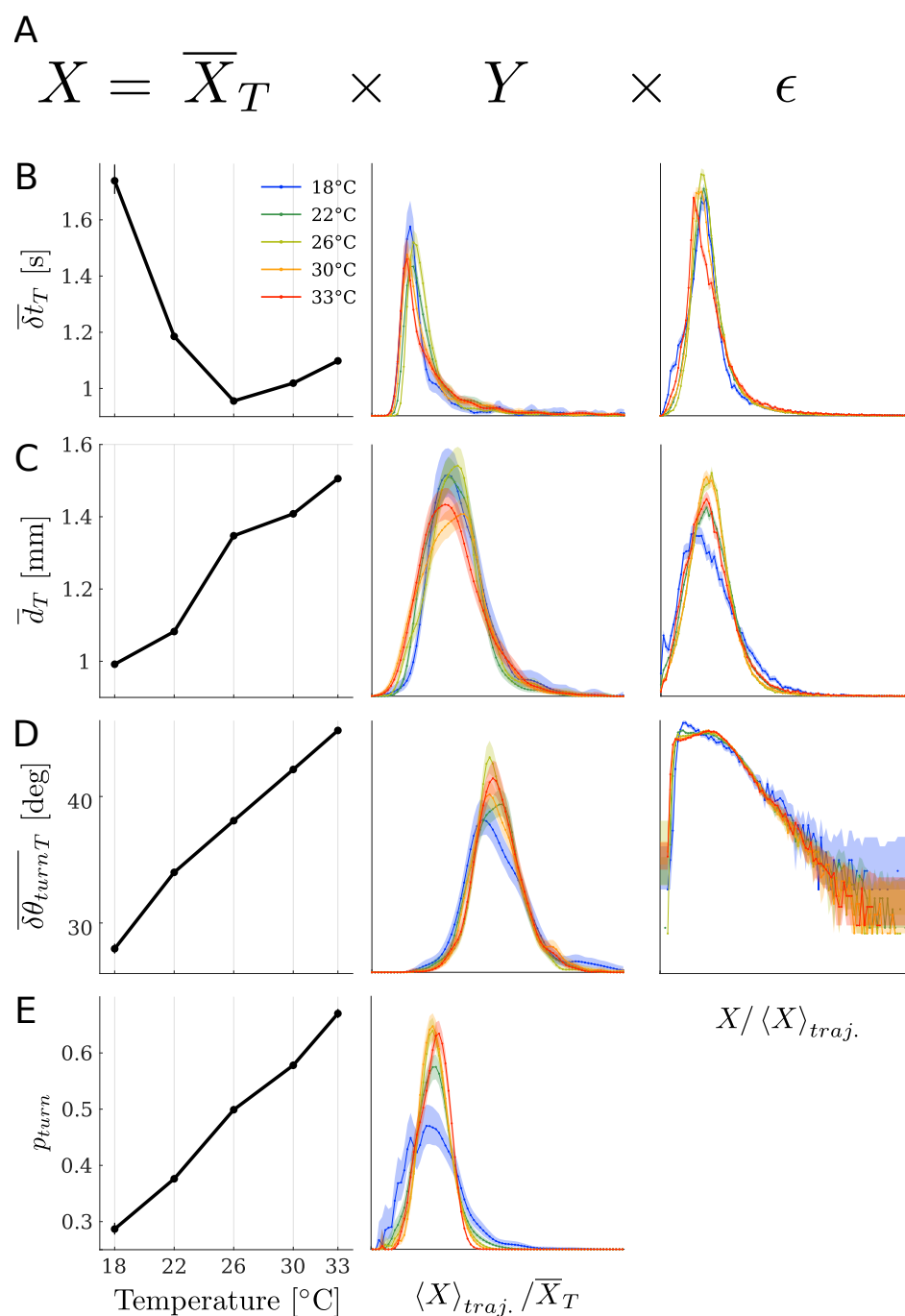


Figure S3: Temperature-independent rescaling of parameters. **A** Equation describing parameter X distribution. **B-E** Left to right, temperature-averaged value, trajectory-averaged rescaled by temperature averaged-value and per-bout value rescaled by the trajectory average, for **B** interbout intervals, **C** displacements, **D** reorientation angle of turn events, **E** turning probability.

MARCH 17, 2021

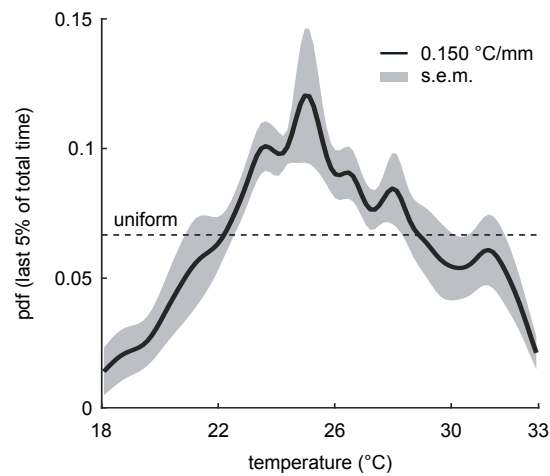


Figure S4: Fish position distributions along a linear thermal gradient. Presence probability density function of 10 batches of 10 larvae experiencing a thermal gradient from 18°C to 33°C. Solid line is the mean across batches, shaded area is the s.e.m. Dashed line is the expected value for a uniform distribution.

530 **References**

- 531 [1] Allison K. Shaw. “Causes and consequences of individual variation in animal movement”. In: *Movement*
532 *Ecology* 8.1 (2020), p. 12. DOI: 10.1186/s40462-020-0197-x.
- 533 [2] João C. Marques, Meng Li, Diane Schaak, Drew N. Robson, and Jennifer M. Li. “Internal state
534 dynamics shape brainwide activity and foraging behaviour”. In: *Nature* 577.7789 (2020), pp. 239–243.
535 DOI: 10.1038/s41586-019-1858-z.
- 536 [3] Robert Evan Johnson, Scott Linderman, Thomas Panier, Caroline Lei Wee, Erin Song, Kristian Joseph
537 Herrera, Andrew Miller, and Florian Engert. “Probabilistic Models of Larval Zebrafish Behavior Reveal
538 Structure on Many Scales”. In: *Current Biology* 30.1 (2020), 70–82.e4. DOI: 10.1016/j.cub.2019.11.
539 026.
- 540 [4] John H. Gillespie. “Natural selection for within-generation variance in offspring number”. In: *Genetics*
541 76.3 (1974). Publisher: Genetics .eprint: <https://www.genetics.org/content/76/3/601.full.pdf>, pp. 601–
542 606.
- 543 [5] Tom Philippi and Jon Seger. “Hedging one’s evolutionary bets, revisited”. In: *Trends in Ecology &*
544 *Evolution* 4.2 (1989), pp. 41–44. DOI: 10.1016/0169-5347(89)90138-9.
- 545 [6] Matthew Lovett-Barron, Aaron S. Andalman, William E. Allen, Sam Vesuna, Isaac Kauvar, Vanessa M.
546 Burns, and Karl Deisseroth. “Ancestral Circuits for the Coordinated Modulation of Brain State”. In:
547 *Cell* 171.6 (2017), 1411–1423.e17. DOI: 10.1016/j.cell.2017.10.021.
- 548 [7] David A. McCormick, Dennis B. Nestvogel, and Biyu J. He. “Neuromodulation of Brain State and
549 Behavior”. In: *Annual Review of Neuroscience* 43.1 (2020), pp. 391–415. DOI: 10.1146/annurev-neuro-
550 100219-105424.
- 551 [8] Stuart W.S. MacDonald, Lars Nyberg, and Lars Bäckman. “Intra-individual variability in behavior:
552 links to brain structure, neurotransmission and neuronal activity”. In: *Trends in Neurosciences* 29.8
553 (2006), pp. 474–480. DOI: 10.1016/j.tins.2006.06.011.
- 554 [9] P. Robin Hiesinger and Bassem A. Hassan. “The Evolution of Variability and Robustness in Neural
555 Development”. In: *Trends in Neurosciences* 41.9 (2018), pp. 577–586. DOI: 10.1016/j.tins.2018.05.
556 007.
- 557 [10] Thomas Panier, Sebastián A. Romano, Raphaël Olive, Thomas Pietri, Germán Sumbre, Raphaël
558 Candelier, and Georges Debrégeas. “Fast functional imaging of multiple brain regions in intact zebrafish
559 larvae using Selective Plane Illumination Microscopy”. In: *Frontiers in Neural Circuits* 7 (2013). DOI:
560 10.3389/fncir.2013.00065.
- 561 [11] Misha B Ahrens, Michael B Orger, Drew N Robson, Jennifer M Li, and Philipp J Keller. “Whole-brain
562 functional imaging at cellular resolution using light-sheet microscopy”. In: *Nature Methods* 10.5 (2013),
563 pp. 413–420. DOI: 10.1038/nmeth.2434.
- 564 [12] Ruben Portugues, Claudia E. Feierstein, Florian Engert, and Michael B. Orger. “Whole-Brain Activity
565 Maps Reveal Stereotyped, Distributed Networks for Visuomotor Behavior”. In: *Neuron* 81.6 (2014),
566 pp. 1328–1343. DOI: 10.1016/j.neuron.2014.01.019.

- 567 [13] Harold A. Burgess and Michael Granato. “Modulation of locomotor activity in larval zebrafish during
568 light adaptation”. In: *Journal of Experimental Biology* 210.14 (2007). Publisher: The Company of
569 Biologists Ltd Section: Research Article, pp. 2526–2539. DOI: 10.1242/jeb.003939.
- 570 [14] H. A. Burgess and M. Granato. “Sensorimotor Gating in Larval Zebrafish”. In: *Journal of Neuroscience*
571 27.18 (2007), pp. 4984–4994. DOI: 10.1523/JNEUROSCI.0615-07.2007.
- 572 [15] Martin Haesemeyer. “Thermoregulation in fish”. In: *Molecular and Cellular Endocrinology* 518 (2020),
573 p. 110986. DOI: 10.1016/j.mce.2020.110986.
- 574 [16] Raymond E. Engeszer, Larissa B. Patterson, Andrew A. Rao, and David M. Parichy. “Zebrafish in
575 The Wild: A Review of Natural History And New Notes from The Field”. In: *Zebrafish* 4.1 (2007),
576 pp. 21–40. DOI: 10.1089/zeb.2006.9997.
- 577 [17] Martin Haesemeyer, Drew N. Robson, Jennifer M. Li, Alexander F. Schier, and Florian Engert. “The
578 Structure and Timescales of Heat Perception in Larval Zebrafish”. In: *Cell Systems* 1.5 (2015), pp. 338–
579 348. DOI: 10.1016/j.cels.2015.10.010.
- 580 [18] Martin Haesemeyer, Drew N. Robson, Jennifer M. Li, Alexander F. Schier, and Florian Engert. “A
581 Brain-wide Circuit Model of Heat-Evoked Swimming Behavior in Larval Zebrafish”. In: *Neuron* 98.4
582 (2018), 817–831.e6. DOI: 10.1016/j.neuron.2018.04.013.
- 583 [19] Sophia Karpenko, Sebastien Wolf, Julie Lafaye, Guillaume Le Goc, Thomas Panier, Volker Bormuth,
584 Raphaël Candelier, and Georges Debrégeas. “From behavior to circuit modeling of light-seeking
585 navigation in zebrafish larvae”. In: *eLife* 9 (2020), e52882. DOI: 10.7554/eLife.52882.
- 586 [20] P. Gau, J. Poon, C. Ufret-Vincenty, C. D. Snelson, S. E. Gordon, D. W. Raible, and A. Dhaka. “The
587 Zebrafish Ortholog of TRPV1 Is Required for Heat-Induced Locomotion”. In: *Journal of Neuroscience*
588 33.12 (2013), pp. 5249–5260. DOI: 10.1523/JNEUROSCI.5403-12.2013.
- 589 [21] S A Budick and D M O’Malley. “Locomotion of larval zebrafish”. In: *The Journal of Experimental*
590 *Biology* (2000), p. 15.
- 591 [22] João C. Marques, Simone Lackner, Rita Félix, and Michael B. Orger. “Structure of the Zebrafish
592 Locomotor Repertoire Revealed with Unsupervised Behavioral Clustering”. In: *Current Biology* 28.2
593 (2018), 181–195.e5. DOI: 10.1016/j.cub.2017.12.002.
- 594 [23] Benjamin Gallois and Raphaël Candelier. “FastTrack: An open-source software for tracking varying
595 numbers of deformable objects”. In: *PLOS Computational Biology* 17.2 (2021), e1008697. DOI: 10.
596 1371/journal.pcbi.1008697.
- 597 [24] Xiuye Chen and Florian Engert. “Navigational strategies underlying phototaxis in larval zebrafish”. In:
598 *Frontiers in Systems Neuroscience* 8 (2014). DOI: 10.3389/fnsys.2014.00039.
- 599 [25] Timothy W Dunn, Yu Mu, Sujatha Narayan, Owen Randlett, Eva A Naumann, Chao-Tsung Yang,
600 Alexander F Schier, Jeremy Freeman, Florian Engert, and Misha B Ahrens. “Brain-wide mapping
601 of neural activity controlling zebrafish exploratory locomotion”. In: *eLife* 5 (2016), e12741. DOI:
602 10.7554/eLife.12741.

- 603 [26] Sébastien Wolf, Alexis M. Dubreuil, Tommaso Bertoni, Urs Lucas Böhm, Volker Bormuth, Raphaël
604 Candelier, Sophia Karpenko, David G. C. Hildebrand, Isaac H. Bianco, Rémi Monasson, and Georges
605 Debrégeas. “Sensorimotor computation underlying phototaxis in zebrafish”. In: *Nature Communications*
606 8.1 (2017), p. 651. DOI: 10.1038/s41467-017-00310-3.
- 607 [27] V. Balakrishnan. *Mathematical Physics: Applications and Problems*. Cham: Springer International
608 Publishing, 2020. DOI: 10.1007/978-3-030-39680-0.
- 609 [28] Henry F. Kaiser. “The Application of Electronic Computers to Factor Analysis”. In: *Educational and*
610 *Psychological Measurement* 20.1 (1960), pp. 141–151. DOI: 10.1177/001316446002000116.
- 611 [29] G. E. Uhlenbeck and L. S. Ornstein. “On the Theory of the Brownian Motion”. In: *Physical Review*
612 36.5 (1930), pp. 823–841. DOI: 10.1103/PhysRev.36.823.
- 613 [30] Crispin W. Gardiner. *Handbook of stochastic methods: for physics, chemistry and the natural sciences*.
614 Study ed., 2. ed., 6. print. Springer series in synergetics 13. OCLC: 174775208. Berlin: Springer, 2002.
615 444 pp.
- 616 [31] John W. Krakauer, Asif A. Ghazanfar, Alex Gomez-Marin, Malcolm A. MacIver, and David Poeppel.
617 “Neuroscience Needs Behavior: Correcting a Reductionist Bias”. In: *Neuron* 93.3 (2017), pp. 480–490.
618 DOI: <https://doi.org/10.1016/j.neuron.2016.12.041>.
- 619 [32] Sandeep Robert Datta, David J. Anderson, Kristin Branson, Pietro Perona, and Andrew Leifer.
620 “Computational Neuroethology: A Call to Action”. In: *Neuron* 104.1 (2019), pp. 11–24. DOI: <https://doi.org/10.1016/j.neuron.2019.09.038>.
621
- 622 [33] Greg J. Stephens, Bethany Johnson-Kerner, William Bialek, and William S. Ryu. “Dimensionality and
623 Dynamics in the Behavior of *C. elegans*”. In: *PLOS Computational Biology* 4.4 (2008), pp. 1–10. DOI:
624 10.1371/journal.pcbi.1000028.
- 625 [34] Kristin Branson, Alice A Robie, John Bender, Pietro Perona, and Michael H Dickinson. “High-
626 throughput ethomics in large groups of *Drosophila*”. In: *Nature Methods* 6.6 (2009), pp. 451–457. DOI:
627 10.1038/nmeth.1328.
- 628 [35] Joshua M. Mueller, Primoz Ravbar, Julie H. Simpson, and Jean M. Carlson. “*Drosophila melanogaster*
629 grooming possesses syntax with distinct rules at different temporal scales”. en. In: *PLOS Computational*
630 *Biology* 15.6 (2019). Ed. by Adam Calhoun, e1007105. DOI: 10.1371/journal.pcbi.1007105.
- 631 [36] Alexander B. Wiltschko, Matthew J. Johnson, Giuliano Iurilli, Ralph E. Peterson, Jesse M. Katon,
632 Stan L. Pashkovski, Victoria E. Abaira, Ryan P. Adams, and Sandeep Robert Datta. “Mapping
633 Sub-Second Structure in Mouse Behavior”. In: *Neuron* 88.6 (2015). Publisher: Elsevier, pp. 1121–1135.
634 DOI: 10.1016/j.neuron.2015.11.031.
- 635 [37] L. Mazzucato, A. Fontanini, and G. La Camera. “Dynamics of Multistable States during Ongoing
636 and Evoked Cortical Activity”. en. In: *Journal of Neuroscience* 35.21 (2015), pp. 8214–8231. DOI:
637 10.1523/JNEUROSCI.4819-14.2015.
- 638 [38] Kristen E. Severi, Ruben Portugues, João C. Marques, Donald M. O’Malley, Michael B. Orger, and
639 Florian Engert. “Neural Control and Modulation of Swimming Speed in the Larval Zebrafish”. In:
640 *Neuron* 83.3 (2014), pp. 692–707. DOI: 10.1016/j.neuron.2014.06.032.

MARCH 17, 2021

- 641 [39] Bertil Hille. *Ion Channels of Excitable Membranes*. 3rd ed. Sinauer Associates, 2001. 814 pp.
- 642 [40] Lamont S. Tang, Adam L. Taylor, Anatoly Rinberg, and Eve Marder. “Robustness of a Rhythmic Circuit
643 to Short- and Long-Term Temperature Changes”. In: *Journal of Neuroscience* 32.29 (2012). Publisher:
644 Society for Neuroscience Section: Articles, pp. 10075–10085. DOI: 10.1523/JNEUROSCI.1443-12.2012.
- 645 [41] Anatoly Rinberg, Adam L. Taylor, and Eve Marder. “The Effects of Temperature on the Stability of a
646 Neuronal Oscillator”. In: *PLOS Computational Biology* 9.1 (2013). Publisher: Public Library of Science,
647 e1002857. DOI: 10.1371/journal.pcbi.1002857.
- 648 [42] R. S. Batty and J. H. S. Blaxter. “The Effect of Temperature on the Burst Swimming Performance of
649 Fish Larvae”. In: *Journal of Experimental Biology* 170.1 (1992). Publisher: The Company of Biologists
650 Ltd Section: Journal Articles, pp. 187–201.
- 651 [43] T. Yokogawa, M. C. Hannan, and H. A. Burgess. “The Dorsal Raphe Modulates Sensory Responsiveness
652 during Arousal in Zebrafish”. In: *Journal of Neuroscience* 32.43 (2012), pp. 15205–15215. DOI: 10.
653 1523/JNEUROSCI.1019-12.2012.
- 654 [44] Eran Lottem, Dhruva Banerjee, Pietro Vertechi, Dario Sarra, Matthijs oude Lohuis, and Zachary F.
655 Mainen. “Activation of serotonin neurons promotes active persistence in a probabilistic foraging task”.
656 In: *Nature Communications* 9.1 (2018), p. 1000. DOI: 10.1038/s41467-018-03438-y.
- 657 [45] Aaron S. Andalman, Vanessa M. Burns, Matthew Lovett-Barron, Michael Broxton, Ben Poole, Samuel J.
658 Yang, Logan Grose, Talia N. Lerner, Ritchie Chen, Tyler Benster, Philippe Mourrain, Marc Levoy,
659 Kanaka Rajan, and Karl Deisseroth. “Neuronal Dynamics Regulating Brain and Behavioral State
660 Transitions”. en. In: *Cell* 177.4 (2019), 970–985.e20. DOI: 10.1016/j.cell.2019.02.037.
- 661 [46] Sébastien Wolf, Guillaume Le Goc, Simona Cocco, Georges Debrégeas, and Rémi Monasson. “Emergence
662 of collective spontaneous neural properties from a datadriven model”. In: *In preparation* (2021).
- 663 [47] Nadine Tarantino, Jean-Yves Tinevez, Elizabeth Faris Crowell, Bertrand Boisson, Ricardo Henriques,
664 Musa Mhlanga, Fabrice Agou, Alain Israël, and Emmanuel Laplantine. “TNF and IL-1 exhibit distinct
665 ubiquitin requirements for inducing NEMO–IKK supramolecular structures”. In: *Journal of Cell Biology*
666 204.2 (2014), pp. 231–245. DOI: 10.1083/jcb.201307172.
- 667 [48] Daniel T. Gillespie. “Exact numerical simulation of the Ornstein-Uhlenbeck process and its integral”.
668 In: *Physical Review E* 54.2 (1996), pp. 2084–2091. DOI: 10.1103/PhysRevE.54.2084.